Letter

Hopfield neural network in magnetic textures with intrinsic Hebbian learning

Weichao Yu (余伟超),[1,2,3,4] Jiang Xiao (萧江),[2,3,4,5,*] and Gerrit E. W. Bauer (包格瑞)[1,6,7]

[1]*Institute for Materials Research, Tohoku University, Sendai 980-8577, Japan*
[2]*State Key Laboratory of Surface Physics and Institute for Nanoelectronic Devices and Quantum Computing, Fudan University, Shanghai 200433, China*
[3]*Shanghai Qi Zhi Institute, Shanghai 200232, China*
[4]*Shanghai Research Center for Quantum Sciences, Shanghai 201315, China*
[5]*Department of Physics and State Key Laboratory of Surface Physics, Fudan University, Shanghai 200433, China*
[6]*WPI-AIMR, Tohoku University, Sendai 980-8577, Japan*
[7]*Zernike Institute for Advanced Materials, University of Groningen, 9747 AG Groningen, Netherlands*

(Received 8 January 2021; revised 1 November 2021; accepted 1 November 2021; published 16 November 2021)

Macroscopic spin ensembles with brainlike features such as nonlinearity, stochasticity, self-oscillations, memory effects, and plasticity, form attractive platforms for neuromorphic computing. We propose an artificial neural network consisting of electric contacts on conducting films with tunable magnetic textures that is superior to conventional implementations, because it does not require resource-demanding external computations during training. Simulations show that the feedback between anisotropic magnetoresistance and current-induced spin-transfer torque in malleable magnetic textures autonomously trains the network according to the Hebbian learning principle. We illustrate the idea by simulating the pattern recognition by a four-node Hopfield neural network.

DOI: 10.1103/PhysRevB.104.L180405

Introduction. Neuromorphic computing is a rapidly developing field in information technology with impressive performance in tasks such as pattern recognitions or language translation. However, von Neumann architectures that emulate brain-inspired algorithms with physically separated computing and storage units are very inefficient. For example, the power consumption of the Alpha Go processor (∼1 MW) is 50 000 times higher than that of a human brain (∼20 W) [1,2]. A sustainable route towards artificial intelligence would be an architecture with hard-wired neuromorphic functions. Spintronic devices share features of the brain, such as nonlinearity, memory, self-oscillations, stochasticity, plasticity, high degrees of freedom, etc. [3]. These advantages already led to alternative computing schemes, such as the stochastic [4,5], in-memory logic [6], as well as neuromorphic computing [7].

The artificial neural network (ANN) is a widely used model for neuromorphic computing, with artificial neurons and synapses that emulate biological system [8]. Neurons are devices with output signals that spike when the integrated input reaches a certain threshold, while synapses connect the neurons with tunable weights. Spintronic devices can mimic both functionalities. For example, spin-torque oscillators can serve as artificial neurons and recognize spoken digits and vowels [9,10]. The nonlinear dynamics of skyrmion fabrics can preprocess information for reservoir computing [11–13].

Memristors with an electric resistance that depends on its history are widely used as artificial synapses [14–17]. Spintronics offers memristor functionalities by reconfigurable magnetic configurations whose resistance depends on, for example, the positions of magnetic domain walls [18], the number of skyrmions [19–21], or the texture in antiferromagnet/ferromagnet bilayers [22], all of which can be controlled by applied fields or currents.

In most software and hardware realizations of an ANN, the weight-updating process of the synapses is based on external algorithms, such as the back-propagation method in which external computations allocate new weights based on the results of a previous cycle. Unfortunately, this is expensive in terms of resource and energy consumption [23]. Here, we propose a platform for neuromorphic computation that can learn "naturally" by itself. The proposed network is based on an electrically conducting magnetic thin film with an inhomogeneous magnetic texture, with weights encoded by the conductance matrix between attached electrodes. Conventionally, weights are updated during the training cycle according to algorithms inspired by Hebb's learning principle [24]: *Cells that fire together wire together*. We propose that this principle can be intrinsically embedded in the dynamic evolution of the magnetic texture under the current-induced spin-transfer torque, hence external intervention and computation are no longer needed [25]. As a proof of principle, we simulate the performance of a four-node Hopfield network on a magnetic thin film with maze spiral domains as shown in Fig. 1(g).

Modeling. The dynamics of the magnetization $\mathbf{M}(\mathbf{r}, t)$ of a ferromagnetic film with saturation magnetization

*xiaojiang@fudan.edu.cn

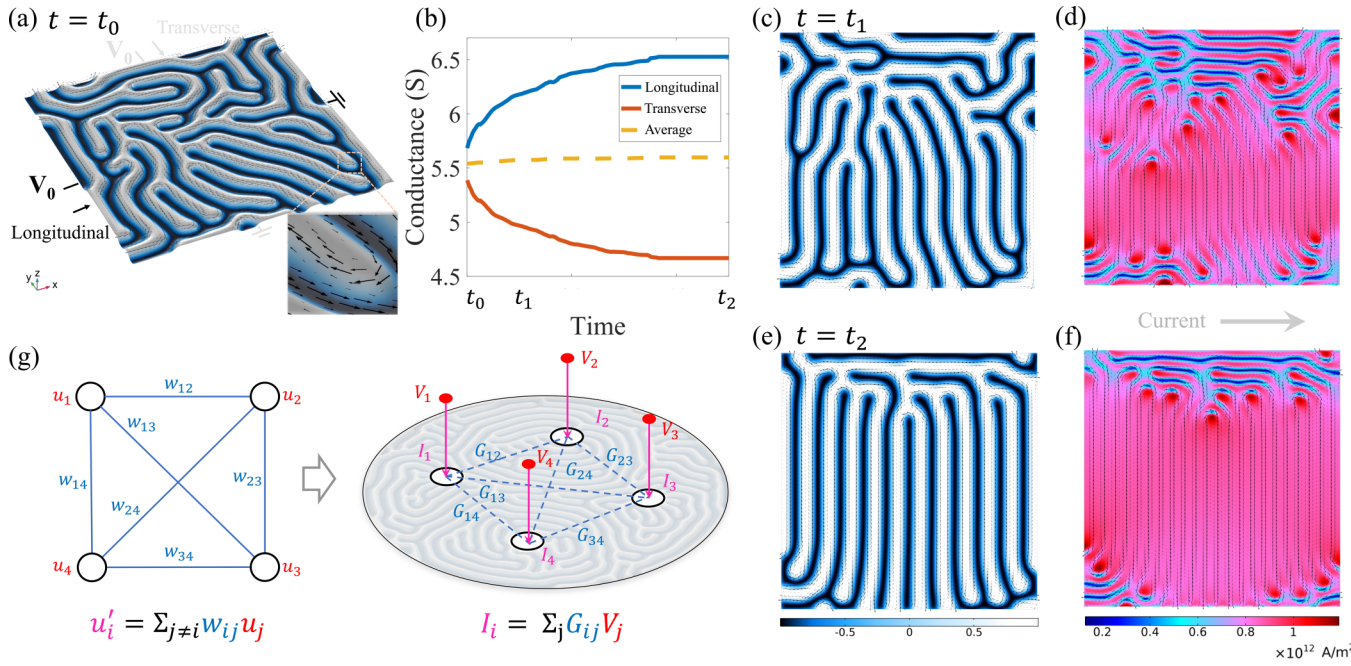

FIG. 1. Magnetic textures with plasticity. (a) Snapshot of a maze domain structure at $t_0 = 0$ ns (color code for out-of-plane magnetization and arrows for in-plane magnetization). (b) Calculated conductance $|G|$ in longitudinal ($\hat{\mathbf{x}}$) and transverse ($\hat{\mathbf{y}}$) directions. Snapshots of magnetization [(c), (e)] and current density $|\mathbf{j}|$ [(d), (f)] distributions at $t_1 = 10$ ns and $t_2 = 50$ ns, respectively. An applied $V_0 = 0.05$ V drives a current along the x direction. (g) Left: Schematical Hopfield network formed by four neurons with values u_i and weights w_{ij}. Right: Implementation of this network by a magnetic thin film with a texture that stores weights that can be trained by currents. The inputs are the voltages V_i at the electrodes and the outputs are the currents I_i into the film. The conductances G_{ij} are equivalent to the weights in the Hopfield network.

M_s is governed by the Landau-Lifshitz-Gilbert (LLG) equation

$$\frac{\partial \mathbf{m}}{\partial t} = -\gamma \mathbf{m} \times \mathbf{H}_{\text{eff}} + \alpha \mathbf{m} \times \frac{\partial \mathbf{m}}{\partial t} + \tau_{\text{d}}, \tag{1}$$

where $\mathbf{m} = \mathbf{M}/M_s$, γ is the gyromagnetic ratio, and α is the Gilbert damping constant. The effective magnetic field

$$\mathbf{H}_{\text{eff}} = A\nabla^2 \mathbf{m} + K\mathbf{m} \cdot \hat{\mathbf{z}} - D\nabla \times \mathbf{m} \tag{2}$$

consists of the exchange interaction, the perpendicular easy-axis anisotropy along $\hat{\mathbf{z}}$, and a bulk-type Dzyaloshinskii-Moriya interaction (DMI) [26–28], parametrized by A, K, and D, respectively. The current-induced spin-transfer torque [29–31] in Eq. (1),

$$\tau_{\text{d}} = \frac{\mu_{\text{B}} P}{e M_s} (\mathbf{j} \cdot \nabla)\mathbf{m}, \tag{3}$$

is proportional to the electric current density $\mathbf{j}$, where μ_{B} is the Bohr magneton, P the (conductivity) spin polarization, and $-e$ the electron charge. The dipolar interaction is not important for the energetics of submicrometer scale textures and may be disregarded for the DMI-stabilized ones considered here.

The electric current density $\mathbf{j}$ is proportional to the local electric field $\mathbf{E}$,

$$\mathbf{j}(\mathbf{r}) = \hat{\Sigma}[\mathbf{m}(\mathbf{r})] \cdot \mathbf{E}(\mathbf{r}), \tag{4}$$

where $\hat{\Sigma}[\mathbf{m}]$ is the 2×2 conductivity matrix of a magnetic thin film with the anisotropic magnetoresistance (AMR) [32], i.e., a local resistivity depending on the angle θ between the current flow and the local magnetization $\mathbf{m}(\mathbf{r})$ as $\rho = \rho_{\parallel} \cos^2\theta + \rho_{\perp} \sin^2\theta$. Inverting this relation, the Cartesian elements $\Sigma_{ij}[\mathbf{m}] = \sigma_{\perp} + \sigma_{\delta} m_i m_j$ with $\sigma_{\perp} = 1/\rho_{\perp}$, $\sigma_{\delta} = 1/\rho_{\parallel} - 1/\rho_{\perp}$ and the AMR ratio $a = 2(\rho_{\parallel} - \rho_{\perp})/(\rho_{\parallel} + \rho_{\perp})$ [11–13,33]. A large enough current-induced torque in Eq. (1) rotates the magnetization that in turn modulates the current distribution by Eq. (4). We solve the spatiotemporal Eqs. (1) and (4) self-consistently under the constraint $\nabla \cdot \mathbf{j} = \mathbf{0}$ by the COMSOL MULTIPHYSICS [34] finite element code.

Magnetic synapse. In magnetic films with DMI, $D > 4\sqrt{AK}/\pi$ [28,35,36], a spiral maze domain texture emerges [37] as illustrated by Fig. 1(a) for a 400 nm × 400 nm slab with thickness 1 μm. Parameters are typical for, e.g., Pt/CoFe/MgO, but combined with a large AMR ratio $a = 150\%$ found in Sr_2IrO_4 [38], and $D = 6.5 \times 10^{-3}$ A. In this system many energetically nearly degenerate textures span a huge configuration space that is accessible by small variations in temperature, field, or voltage. Here, we focus on the overdamped regime with $\alpha = 0.3$, which can be reached by rare earth doping [39]. The low-energy realizations of magnetic textures are then stable in the absence of applied torque and forces and the effects of weak pinning may be disregarded [see Supplemental Material (SM) [40]].

Under the action of the spin-transfer torque caused by an electric voltage V_0 applied across the film, the texture and its conductance evolve with time. Figures 1(c)–1(f) show snapshots for $V_0 = 0.05$ V applied in the x direction, as in Fig. 1(a). The domains tend to align perpendicular to the current flow to minimize the spin-transfer torque, as observed in thin films of lanthanum strontium manganite [41] and MgO/CoFeB/Pt multilayers [42], but the sample boundaries

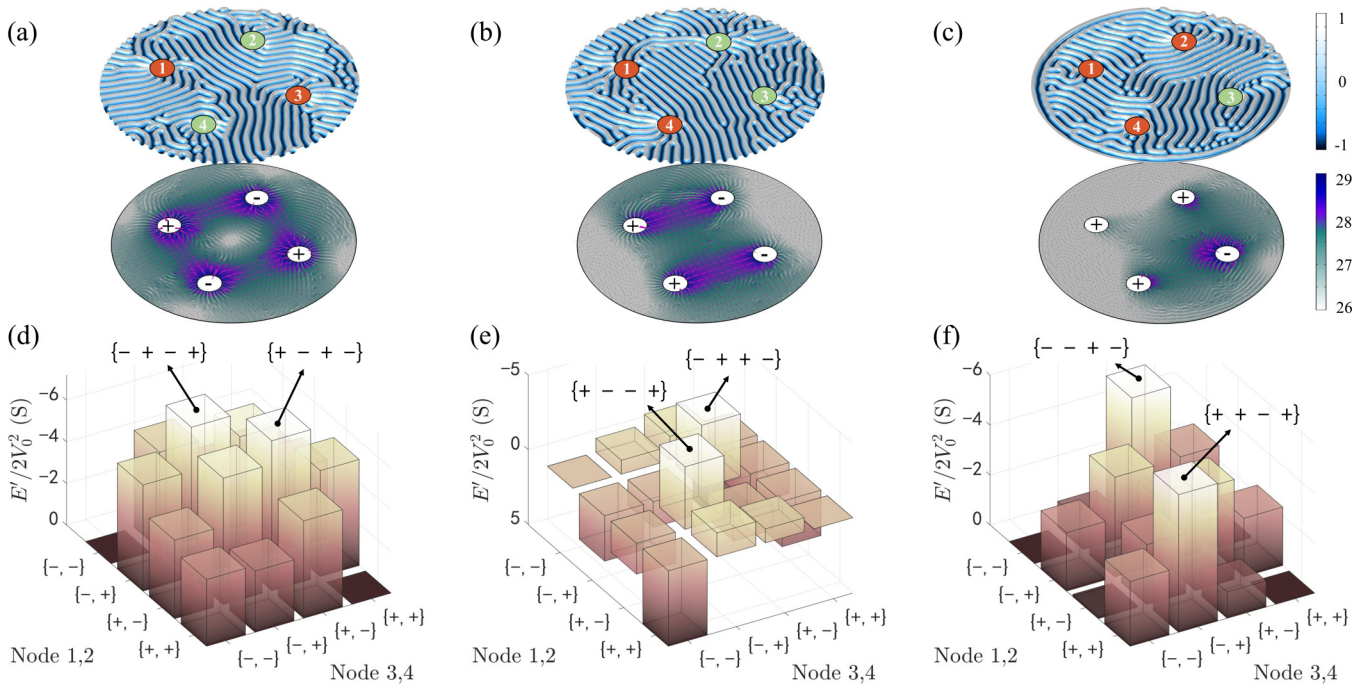

FIG. 2. Trained four-node Hopfield network. The memorized patterns are $\{V_i\} = \{+-+-\}$, $\{+--+\}$, and $\{++-+\}$, respectively. (a)–(c) Magnetization distribution (top panel, arrows for in-plane magnetization and color code for out-of-plane magnetization) and current density distribution $\log|\mathbf{j}|$ (bottom panel, magenta cones for electric current $\mathbf{j}$ on a logarithmic scale). (d)–(f) The effective energy E' [Eq. (7)] is minimal for the trained voltage patterns.

prevent perfect alignment. The current-induced reorientation of the texture increases/decreases the conductance in the longitudinal ($\hat{\mathbf{x}}$)/transverse ($\hat{\mathbf{y}}$) direction, as seen in Fig. 1(b). The magnetic texture acts as memristors that saturate only when high voltages are applied for a sufficiently long time.

A self-learning Hopfield network. The magnetic textures equipped with electrodes establish a Hopfield network [43,44] of fully connected neurons that can recognize patterns. Figure 1(g) sketches a Hopfield network with four neurons connected by the underlying magnetic film. The neuron inputs are the voltages at the electrodes, which we adopt to be binary $\{V_i = \pm V_0\}$. According to Kirchhoff's law $I_i = \sum_j G_{ij}[\mathbf{m}]V_j$, the current through the electrodes is governed by a (symmetric) conductance matrix $G_{ij}[\mathbf{m}] = G^0_{ij} + G'_{ij}[\mathbf{m}]$ with texture-independent $\hat{G}_0$ and dependent $\hat{G}'$ contributions [45]. Current conservation requires

$$G_{ii} = -\sum_{j\neq i} G_{ij} > 0 \quad \text{with} \quad G_{ij} < 0 \quad \text{for} \quad i \neq j, \tag{5}$$

where a current is positive when flowing into the electrodes. $\hat{G}_0$ can be measured by saturating the magnetic film by a sufficiently strong magnetic field perpendicular to the film and satisfies the same constraints as $\hat{G}$ in Eq. (5). The difference $\hat{G}' = \hat{G} - \hat{G}_0$ is still bound by $G'_{ii} = -\sum_{j\neq i} G'_{ij}$ but the nondiagonal elements G'_{ij} can have either sign.

We may distinguish the current contributions from $\hat{G}_0$ and $\hat{G}'$: $I_i = I^0_i + I'_i$, where

$$I'_i = \sum_j G'_{ij}V_j. \tag{6}$$

This completes the formulation of the Hopfield network with $V_j = \pm V_0$ the neuron inputs, G'_{ij} the tunable weights, and $\mathrm{sgn}(I'_i)$ the neuron outputs. Analogous to the the bipolar Ising spin glass model [46], we define the functional energy

$$E' = -\sum_i I'_i V_i = -\sum_{i,j} G'_{ij}V_iV_j = 2V_0^2 \sum_{V_i\neq V_j} G'_{ij}. \tag{7}$$

Physically, $-E'$ is the power consumption for a conductance matrix G_{ij} relative to that of the texture-free thin film (G^0_{ij}): $-E' = -E - (-E_0)$ with $-E_0 = \sum_i G^0_{ij}V_iV_j$. With fixed G^0_{ij}, we know $-E_0$ in advance for arbitrary inputs $\{V_i\}$. The energy Eq. (7) therefore measures the additional Joule heating caused by the magnetic texture.

The film can be trained to memorize a pattern encoded by an array of binary values $\mathbf{V} \equiv \{V_i\}$ simply by letting the magnetization evolve under the voltages $\{V_i\}$. The texture adjusts itself to the current-induced spin-transfer torque such that the conductances ($|G_{ij}|$ and $|G'_{ij}|$) between electrode i and j increase when $V_i \neq V_j$, thereby decreasing the objective function E' in Eq. (7). The conductances between electrodes with the same voltage cannot be directly trained, but they tend to decrease when other conductances grow.

Figure 2 shows examples of a four-neuron network that was trained to memorize three patterns that were imprinted by voltage distributions over the nodes as $\{+-+-\}$, $\{+--+\}$, $\{++-+\}$, respectively. The top panels show the post-training texture and current density distributions. The lower panels of Fig. 2 show the energies Eq. (7) of the trained texture when fed by all possible inputs. The energy is minimized when the trial pattern (up to a global sign change) agrees with

the memorized pattern. For instance, Fig. 2(d) shows clear minima for the equivalent $\{+-+-\}$ and $\{-+-+\}$ states. Due to the point (rotating the pattern according to center) and mirror symmetry (flipping the voltage sign), there are eight degenerate patterns for Fig. 2(c) [two for Fig. 2(a), four for Fig. 2(b)], representing 14 out of 16 possible states (that include the trivial $\{++++\}$ and $\{----\}$) spanned by a four-node Hopfield network.

The memorized pattern can be retrieved by standard inferring algorithms, for example by feeding the neurons with a random initial pattern of binary voltages $\{V_i(0)\}$ with small amplitudes that do not perturb the texture. The voltages can be then updated either asynchronously or synchronously [44] with $V_i(t+1) = \mathrm{sgn}[I_i'(t)]V_0$, where the sign function serves as an activation function which introduces nonlinearity to the network. The self-consistent state with $V_i = \mathrm{sgn}(I_i')V_0$ corresponds to the minimum of the energy function Eq. (7) and the memorized pattern [40].

Intrinsic Hebbian learning. In other types of hardware-implemented synapses, such as cross-bar grid memristors [47,48], the weight-updating requires learning algorithms (such as the back-propagation method) [49] that have to be executed externally. In contrast, the weight updating in magnetic textures does not require any external interference but happens automatically via a positive feedback mechanism between the training current and the texture response. The reinforcement of the interconnection of two neurons by a voltage difference is analogous to Hebb's learning rule in neuroscience [24] that simultaneous activation of neurons leads to increased synaptic strength.

By dividing the continuous training process into discrete temporal slices, i.e., regarding the voltages as a train of pulses, the conductance (weight) matrix evolves as

$$G_{ij}^{n+1} = G_{ij}^{n} + \Delta_{ij}^{n}[\{V_i\}]. \tag{8}$$

Here, Δ_{ij}^{n} updates at step-n the weight for the connection between node i and j, depending mainly on the voltage difference $V_i - V_j$, leading to a monotonous increase of weight. The plasticity alone required by Hebbian learning is typically unstable [50], since either all weights may grow to a maximum or decay to a minimum. However, the conductance matrix in the proposed network will not reach overall saturation since the magnetic strips twist and move but cannot be easily created or destroyed, especially in the presence of topological defects stabilized by the DMI. The strengthening of certain connections therefore weakens others, e.g., seen in Fig. 1(b). This competition of the weight modulations replicates another typical feature of organic synapses [44,50,51].

Discussion. We treat the conductance difference $\hat{G}'$ as synaptic weight, hence we infer by the current difference I_i', which is facilitated by a large AMR ratio a. In $Ni_{80}Fe_{20}$ thin films $a \sim 8\%$ [52], $-10\%/6\%$ in single-crystalline Co_xFe_{1-x} alloys depending on growth direction concentration x [53], and $\sim$80% in bilayered $La_{1.2}Sr_{1.8}Mn_2O_7$ single crystals [54]. In antiferromagnetic Sr_2IrO_4 it can reach $a \sim -160\%$ [38]. A larger DMI than used here ($>0.002\,\mathrm{J}/m^2$) reduces the pitch of the spirals and improves the efficiency of the spin-transfer torque. The parameters and voltages are chosen optimistically to keep computation times manageable. The general idea works for less optimal materials, but at the costs of higher power dissipation and training times. We show in the SM that the planar and anomalous Hall effects [40,55] may be disregarded because the in-plane and perpendicular magnetizations vanish on average in the absence of an external field [56].

The bulk-type DMI considered above generates Bloch-type domain walls, that the current induced torque tends to realign such that the conductance increases. In materials with a dominant fieldlike spin-transfer torque [31] or with interfacial-type DMI [28,57], a negative feedback reduces the conductance by applying currents (see SM [40]). Our network scheme can cooperate as well with such negative feedback by swapping the roles of voltage and current in the inferring process and using the resistance instead of conductance as weights in the objective function.

Our proof-of-principle device can only store a 4-pixel pattern. Larger pictures can be stored by increasing the number of nodes, e.g., with positions mimicking the locations of physical pixels (see SM [40]). Scaling up the network increases the storing capacity in the form of more complex and multiple input patterns, and multiple patterns can be memorized when the energy function has multiple local minima [43]. The performance can be optimized also by flexible node positions and/or three-dimensional textures.

Conclusion. We proposed a neural network formed by electric contacts to conducting magnets with a complex magnetization texture. Because of the plasticity of the magnetic textures, the weights of the synapses can be automatically updated during the training process via a positive feedback mechanism between the current-induced spin-transfer torque and the electrical conductance. At the same time, the increase of synaptic weights is constrained by the AMR effect of chiral magnetization texture induced by DMI. We numerically simulate training of and retrieval from a four-node Hopfield network. The concept works also for other types of neural networks and other materials with both "plasticity" and "competence," such as reconfigurable ferroelectrics with conducting domain walls [58,59] and conducting nanowire networks [60]. Our work paves the way to realize hardware-based neuromorphic computing with intrinsic Hebbian learning.

*Acknowledgments.*We are grateful to Shunsuke Fukami, Hangwen Guo, Zhe Yuan, and Ke Xia for fruitful discussions. This work was supported by the JSPS Kakenhi (Grants No. 20K14369 and No. 19H00645). J.X. was supported by National Science Foundation of China (Grant No. 11722430), Shanghai Municipal Science and Technology Major Project (Grant No. 2019SHZDZX01) and Science and Technology Commission of Shanghai Municipality (Grant No. 20JC1415900). W.Y. acknowledges the support from the State Key Laboratory of Surface Physics.

[1] J. Mattheij, Another way of looking at Lee Sedol vs AlphaGo, https://jacquesmattheij.com/another-way-of-looking-at-lee-sedol-vs-alphago/, accessed 17 March 2016.

[2] E. Goi, Q. Zhang, X. Chen, H. Luan, and M. Gu, PhotoniX **1**, 3 (2020).

[3] J. Grollier, D. Querlioz, and M. D. Stiles, Proc. IEEE **104**, 2024 (2016).

[4] W. A. Borders, A. Z. Pervaiz, S. Fukami, K. Y. Camsari, H. Ohno, and S. Datta, Nature (London) **573**, 390 (2019).

[5] M. W. Daniels, A. Madhavan, P. Talatchian, A. Mizrahi, and M. D. Stiles, Phys. Rev. Appl. **13**, 034016 (2020).

[6] W. Yu, J. Lan, and J. Xiao, Phys. Rev. Appl. **13**, 024055 (2020).

[7] J. Grollier, D. Querlioz, K. Y. Camsari, K. Everschor-Sitte, S. Fukami, and M. D. Stiles, Nat. Electron. **3**, 360 (2020).

[8] B. Kröse and P. Smagt, *An Introduction to Neural Networks* (The University of Amsterdam, Amsterdam, 1993).

[9] J. Torrejon, M. Riou, F. A. Araujo, S. Tsunegi, G. Khalsa, D. Querlioz, P. Bortolotti, V. Cros, K. Yakushiji, A. Fukushima, H. Kubota, S. Yuasa, M. D. Stiles, and J. Grollier, Nature (London) **547**, 428 (2017).

[10] M. Romera, P. Talatchian, S. Tsunegi, F. A. Araujo, V. Cros, P. Bortolotti, J. Trastoy, K. Yakushiji, A. Fukushima, H. Kubota, S. Yuasa, M. Ernoult, D. Vodenicarevic, T. Hirtzlin, N. Locatelli, D. Querlioz, and J. Grollier, Nature (London) **563**, 230 (2018).

[11] D. Prychynenko, M. Sitte, K. Litzius, B. Krüger, G. Bourianoff, M. Kläui, J. Sinova, and K. Everschor-Sitte, Phys. Rev. Appl. **9**, 014034 (2018).

[12] G. Bourianoff, D. Pinna, M. Sitte, and K. Everschor-Sitte, AIP Adv. **8**, 055602 (2018).

[13] D. Pinna, G. Bourianoff, and K. Everschor-Sitte, Phys. Rev. Appl. **14**, 054020 (2020).

[14] D. Ielmini and V. Milo, J. Comput. Electron. **16**, 1121 (2017).

[15] M. A. Zidan, J. P. Strachan, and W. D. Lu, Nat. Electronics **1**, 22 (2018).

[16] B. Rajendran and F. Alibart, IEEE Trans. Emerg. Sel. Topics Circuits Syst. **6**, 198 (2016).

[17] S. Yu, Proc. IEEE **106**, 260 (2018).

[18] S. Lequeux, J. Sampaio, V. Cros, K. Yakushiji, A. Fukushima, R. Matsumoto, H. Kubota, S. Yuasa, and J. Grollier, Sci. Rep. **6**, 31510 (2016).

[19] Y. Huang, W. Kang, X. Zhang, Y. Zhou, and W. Zhao, Nanotechnology **28**, 08LT02 (2017).

[20] S. Li, W. Kang, Y. Huang, X. Zhang, Y. Zhou, and W. Zhao, Nanotechnology **28**, 31LT01 (2017).

[21] X. Chen, W. Kang, D. Zhu, X. Zhang, N. Lei, Y. Zhang, Y. Zhou, and W. Zhao, Nanoscale **10**, 6139 (2018).

[22] S. Fukami and H. Ohno, J. Appl. Phys. **124**, 151904 (2018).

[23] R. Ceron, AI today: Data, training and inferencing, https://www.ibm.com/blogs/systems/ai-today-data-training-and-inferencing/ (2019).

[24] A. Hartstein and R. H. Koch, in *Advances in Neural Information Processing Systems 1*, edited by D. S. Touretzky (Morgan-Kaufmann, Burlington, MA, 1989), pp. 769–776.

[25] M. Stern, D. Hexner, J. W. Rocks, and A. J. Liu, Phys. Rev. X **11**, 021045 (2021).

[26] I. Dzyaloshinsky, J. Phys. Chem. Solids **4**, 241 (1958).

[27] T. Moriya, Phys. Rev. **120**, 91 (1960).

[28] S. Rohart and A. Thiaville, Phys. Rev. B **88**, 184422 (2013).

[29] M. D. Stiles and A. Zangwill, Phys. Rev. B **66**, 014407 (2002).

[30] Z. Li and S. Zhang, Phys. Rev. Lett. **92**, 207203 (2004).

[31] S.-M. Seo, K.-J. Lee, H. Yang, and T. Ono, Phys. Rev. Lett. **102**, 147202 (2009).

[32] W. Thomson, Proc. R. Soc. London **8**, 546 (1857).

[33] B. Krüger, Current-driven magnetization dynamics: Analytical modeling and numerical simulation, Ph.D. dissertation, Universität Hamburg, 2012.

[34] COMSOL Multiphysics® version 5.4, www.comsol.com.

[35] S. Woo, K. Litzius, B. Krüger, M.-Y. Im, L. Caretta, K. Richter, M. Mann, A. Krone, R. M. Reeve, M. Weigand, P. Agrawal, I. Lemesh, M.-A. Mawass, P. Fischer, M. Kläui, and G. S. D. Beach, Nat. Mater. **15**, 501 (2016).

[36] J. Lan, W. Yu, and J. Xiao, Nat. Commun. **8**, 178 (2017).

[37] M. Viret, Y. Samson, P. Warin, A. Marty, F. Ott, E. Søndergård, O. Klein, and C. Fermon, Phys. Rev. Lett. **85**, 3962 (2000).

[38] H. Wang, C. Lu, J. Chen, Y. Liu, S. L. Yuan, S.-W. Cheong, S. Dong, and J.-M. Liu, Nat. Commun. **10**, 2280 (2019).

[39] G. Woltersdorf, M. Kiessling, G. Meyer, J.-U. Thiele, and C. H. Back, Phys. Rev. Lett. **102**, 257602 (2009).

[40] See Supplemental Material at http://link.aps.org/supplemental/10.1103/PhysRevB.104.L180405 for details of the numerical method, material parameters, discussion on pinning sites, demonstration of the inferring process, and more supporting data.

[41] C. Liu, S. Wu, J. Zhang, J. Chen, J. Ding, J. Ma, Y. Zhang, Y. Sun, S. Tu, H. Wang, P. Liu, C. Li, Y. Jiang, P. Gao, D. Yu, J. Xiao, R. Duine, M. Wu, C.-W. Nan, J. Zhang *et al.*, Nat. Nanotechnol. **14**, 691 (2019).

[42] I. Lemesh, K. Litzius, M. Böttcher, P. Bassirian, N. Kerber, D. Heinze, J. Zázvorka, F. Büttner, L. Caretta, M. Mann, M. Weigand, S. Finizio, J. Raabe, M.-Y. Im, H. Stoll, G. Schütz, B. Dupé, M. Kläui, and G. S. D. Beach, Adv. Mater. **30**, 1805461 (2018).

[43] J. J. Hopfield, Proc. Natl. Acad. Sci. USA **79**, 2554 (1982).

[44] R. Rojas, *Neural Networks: A Systematic Introduction* (Springer, Berlin, 2013).

[45] Note that $\hat{G}$ is the effective conductance matrix between nodes, while $\hat{\Sigma}$ is a local conductivity matrix.

[46] D. J. Amit, H. Gutfreund, and H. Sompolinsky, Phys. Rev. A **32**, 1007 (1985).

[47] K.-H. Kim, S. Gaba, D. Wheeler, J. M. Cruz-Albrecht, T. Hussain, N. Srinivasa, and W. Lu, Nano Lett. **12**, 389 (2012).

[48] M. Prezioso, F. Merrikh-Bayat, B. D. Hoskins, G. C. Adam, K. K. Likharev, and D. B. Strukov, Nature (London) **521**, 61 (2015).

[49] S. G. Hu, Y. Liu, Z. Liu, T. P. Chen, J. J. Wang, Q. Yu, L. J. Deng, Y. Yin, and S. Hosaka, Nat. Commun. **6**, 7522 (2015).

[50] K. D. Miller and D. J. C. MacKay, Neural Comput. **6**, 100 (1994).

[51] S. Song, K. D. Miller, and L. F. Abbott, Nat. Neurosci. **3**, 919 (2000).

[52] T. G. S. M. Rijks, S. K. J. Lenczowski, R. Coehoorn, and W. J. M. de Jonge, Phys. Rev. B **56**, 362 (1997).

[53] F. L. Zeng, Z. Y. Ren, Y. Li, J. Y. Zeng, M. W. Jia, J. Miao, A. Hoffmann, W. Zhang, Y. Z. Wu, and Z. Yuan, Phys. Rev. Lett. **125**, 097201 (2020).

[54] W. Ning, Z. Qu, Y.-M. Zou, L.-S. Ling, L. Zhang, C.-Y. Xi, H.-F. Du, R.-W. Li, and Y.-H. Zhang, Appl. Phys. Lett. **98**, 212503 (2011).

[55] N. Nagaosa, J. Sinova, S. Onoda, A. H. MacDonald, and N. P. Ong, Rev. Mod. Phys. **82**, 1539 (2010).

[56] T. Taniguchi, J. Grollier, and M. D. Stiles, Phys. Rev. Appl. **3**, 044001 (2015).

[57] A. Fert, V. Cros, and J. Sampaio, Nat. Nanotechnol. **8**, 152 (2013).

[58] D. Meier, J. Seidel, A. Cano, K. Delaney, Y. Kumagai, M. Mostovoy, N. A. Spaldin, R. Ramesh, and M. Fiebig, Nat. Mater. **11**, 284 (2012).

[59] J. P. V. McConville, H. Lu, B. Wang, Y. Tan, C. Cochard, M. Conroy, K. Moore, A. Harvey, U. Bangert, L.-Q. Chen, A. Gruverman, and J. M. Gregg, Adv. Funct. Mater. **30**, 2000109 (2020).

[60] H. G. Manning, F. Niosi, C. G. d. Rocha, A. T. Bellew, C. O'Callaghan, S. Biswas, P. F. Flowers, B. J. Wiley, J. D. Holmes, M. S. Ferreira, and J. J. Boland, Nat. Commun. **9**, 3219 (2018).